Supplementary materials

Temperature Dependent Phase Segregation and morphology evolution in $Ca_{1-x}Ba_xF_2$ Solid Solution grown on Si(001) with an Epitaxial CaF_2 Sublayer

Kaveev A.K. [1,2]*, Alexeev E.A.[1], Belyakova E.I.[1], Yusupova Sh. A.[1], Miniv D.V.[2]

[1] *Ioffe Institute, 194021 St. Petersburg, Russia*

[2] *Alferov University, 194021 St. Petersburg, Russia*

To verify the long-term stability, additional XRD measurements were carried out on sample No. 3, i.e. $Ca_{0.625}Ba_{0.375}F_2$ (growth T = 200°C)/CaF_2/Si(001). The reciprocal space map obtained after 9 months of sample storage fully coincided with that measured on the day of sample creation. The mirror 002 (Fig. S1) and 004 reflections, as well as the side 113, 111, and 222 reflections, remained unchanged in both position and intensity. No additional reflections associated with secondary phases, peak shifts, or intensity variations were observed. Therefore, we conclude that the $Ca_{0.625}Ba_{0.375}F_2$ solid solution remains stable for at least 9 months after growth.

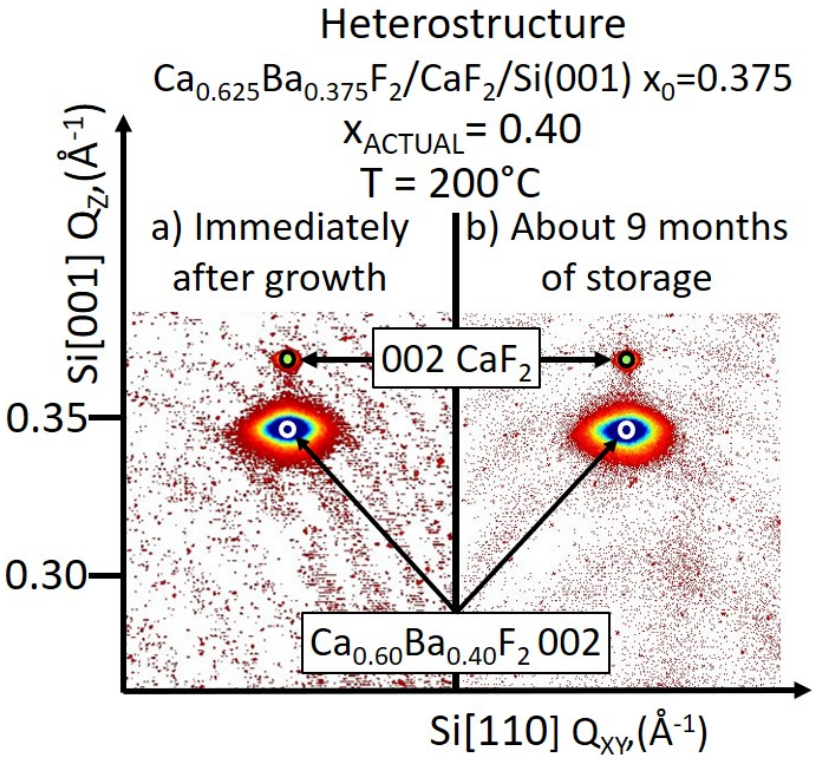

Fig. S1. Comparison of diffraction maps of $Ca_{0.625}Ba_{0.375}F_2$(growth T = 200°C)/CaF_2/Si(001) heterostructure in the region of the forbidden Si(001) reflection: a) diffraction map recorded on

the day of growth, b) diffraction map recorded after 9 months of sample storage at room temperature indoors, without exposure to sunlight, at a relative humidity of approximately 40%.

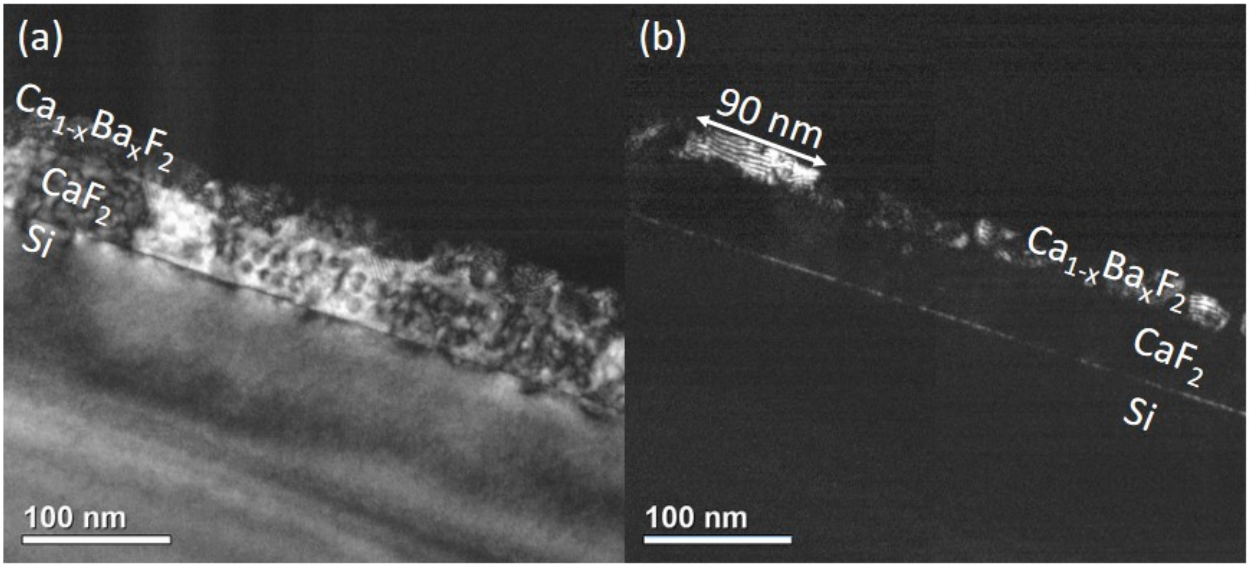

Fig. S2. Dark-field TEM maps of the $Ca_{1-x}Ba_xF_2/CaF_2/Si(001)$ heterostructure: (a) - map acquired under diffraction conditions providing enhanced contrast from the CaF_2 layer; (b) - map acquired under diffraction conditions providing enhanced contrast from the $Ca_{1-x}Ba_xF_2$ layer.

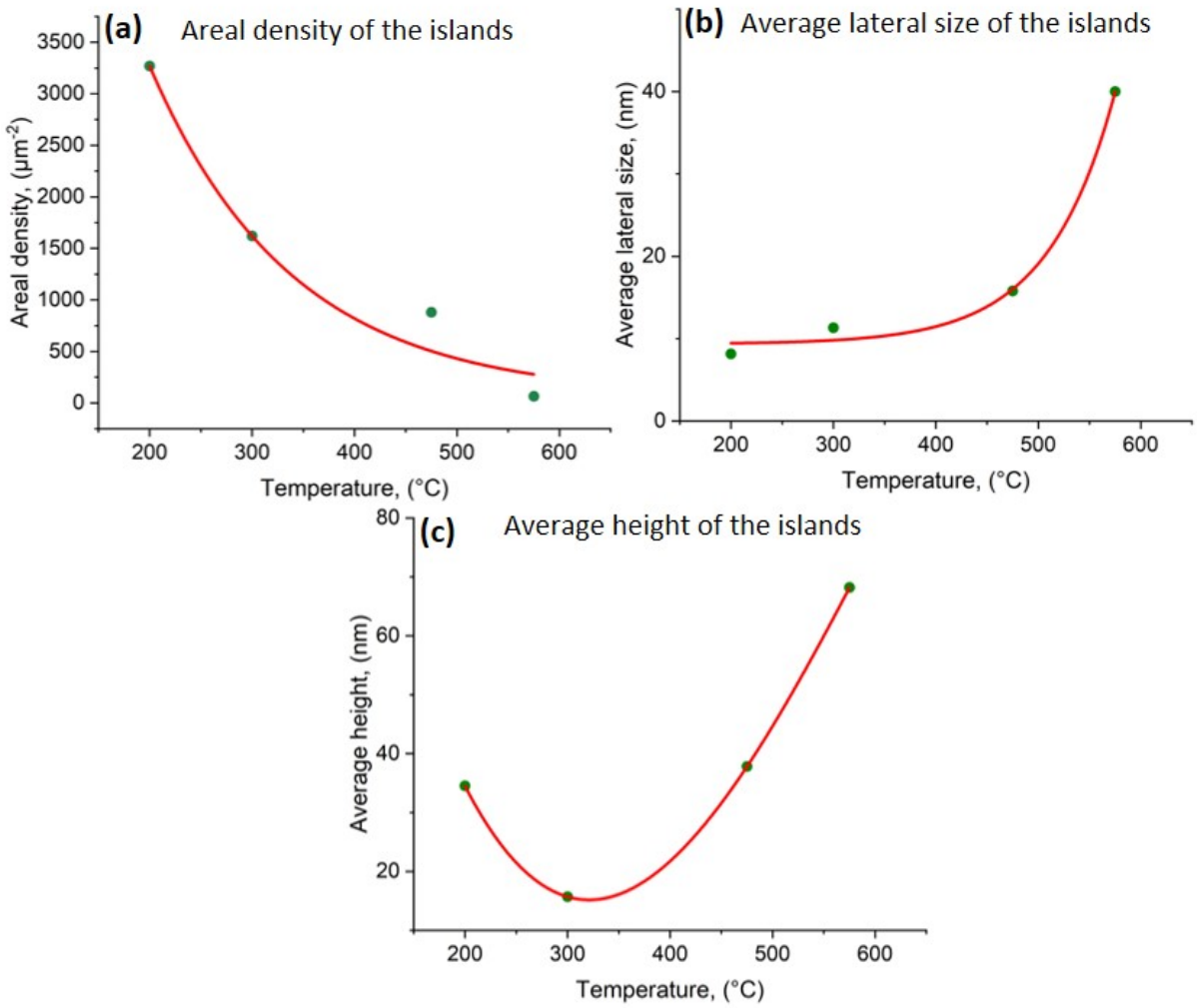

Fig. S3. Dependencies of island density per unit surface area (a), average lateral size (b), and average island height (c) on growth temperature.

The obtained results allow us to draw a qualitative conclusion regarding the effect of growth temperature on the local distribution of barium. Specifically, with increasing temperature from 200 to 575 °C, a redistribution of Ba into localized regions is observed (see Fig. S4, upper images). This shows that an increase in temperature leads to the formation of barium-enriched regions, indicating a reduction in the compositional uniformity of the solid solution at elevated temperatures. To describe the effect of temperature more precisely and to obtain quantitative characteristics, TEM–EDX elemental mapping (Fig. S5) and dark-field TEM measurements (Fig. S2) are presented.

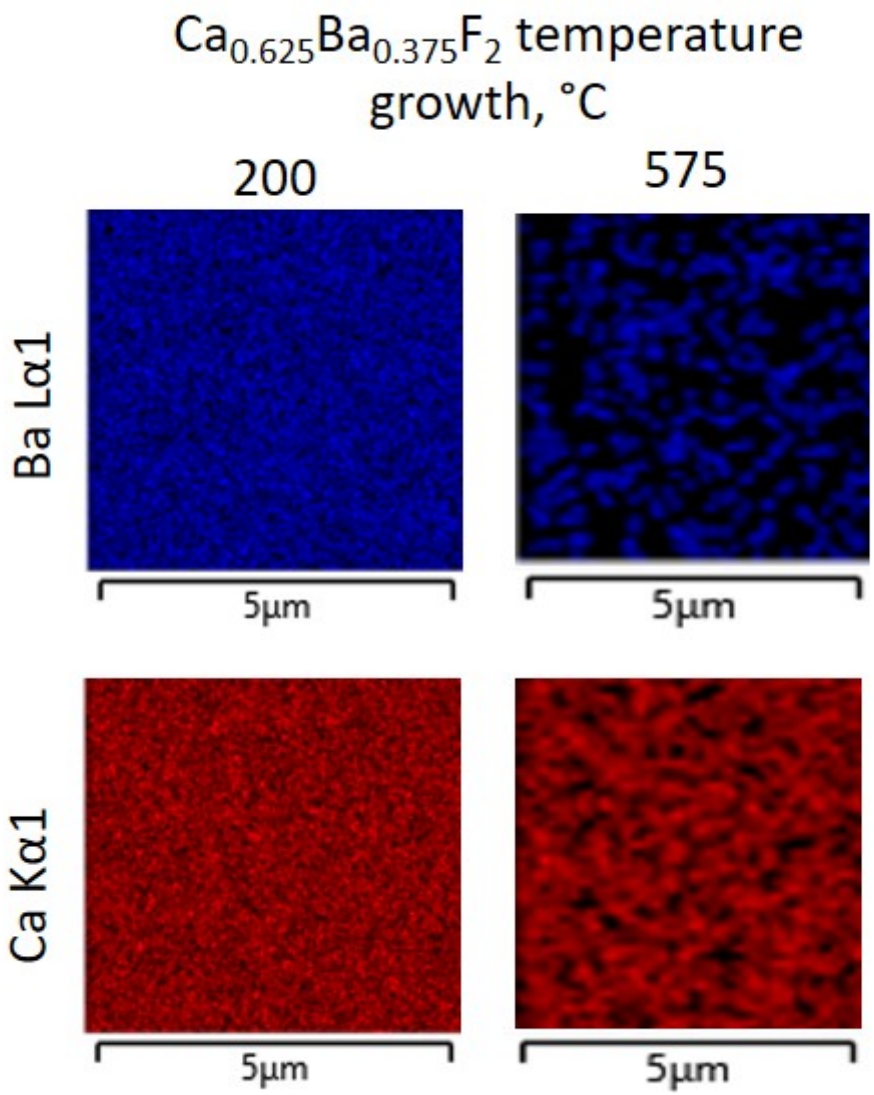

Fig. S4. SEM-EDX elemental maps of $Ca_{1-x}Ba_xF_2$ solid-solution samples grown at 200 and 575 °C. Upper images – Ba distribution map, down images – Ca distribution map.

Fig. S5 presents TEM–EDX elemental mapping of the $Ca_{1-x}Ba_xF_2/CaF_2/Si(001)$ heterostructure with SS growth at 475 °C in a side view. Red circles indicate calcium-depleted regions (Fig. S5, Ca Kα1) or, conversely, barium-enriched regions (Fig. S5, Ba Lα1), as well as the composition of these two regions (Fig. S5, Si-Ca-Ba elemental map composition). These measurements confirm the aforementioned results regarding the local redistribution, showing regions barium-enriched regions and, simultaneously, calcium-depleted regions.

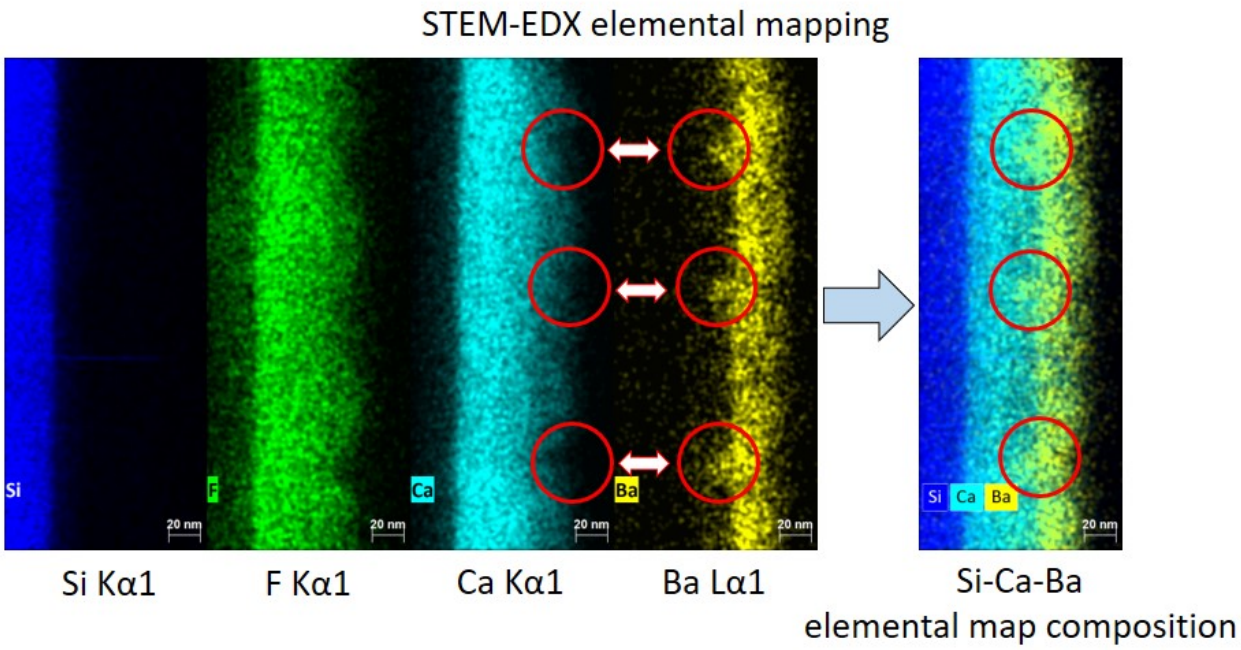

Fig. S5. TEM-EDX maps of $Ca_{1-x}Ba_xF_2$ solid-solution sample grown at 475°C. Distribution maps from left to right: Si, F, Ca, Ba, and the combined Si–Ca–Ba distribution map.

For a quantitative description of the distribution of barium and calcium in the $Ca_{1-x}Ba_xF_2$ layer within this local region, five-point measurements were performed, and the mean value of x, standard deviation (σ), and relative standard deviation (RSD) were calculated (Table S1). One of the measured points, x = 0.20 ± 0.01, agrees well with the XRD value of x = 0.19 for the SS phase $Ca_{1-x}Ba_xF_2$. The mean value, x = 0.26, insignificantly deviates from the value predicted by Vegard's law, probably due to the specific local distribution in this region, as well as the partial influence of the BaF_2 (001) and BaF_2 (111) phases.

№	$Ca_{1-x}Ba_xF_2$		mean x	σ	RSD
	1-x	x			
1	0.73±0.01	0.27±0.01	0.26	0.05	20%
2	0.69±0.01	0.31±0.01			
3	0.80±0.01	0.20±0.01			
4	0.68±0.01	0.32±0.01			
5	0.78±0.01	0.22±0.01			

Table S1. TEM–EDX point measurements, with the calculated mean value of x, standard deviation (σ), and relative standard deviation (RSD).

Dark-field TEM measurements were also performed (Fig. S2). In the first dark-field image (Fig. S2 (a)), the diffraction conditions were adjusted such that the highest intensity corresponded to the CaF_2 layer, whose lattice parameter is close to that of silicon (5.46 and 5.43 Å, respectively). As a result, three distinct layers can be identified in this map: the Si substrate, CaF_2 buffer layer and, partially, the $Ca_{1-x}Ba_xF_2$ SS layer.

In the second image (Fig. S2 (b)), the diffraction conditions were selected to maximize the intensity from a material with a lattice parameter close to that of BaF_2. Under these conditions, contrast is observed exclusively within the $Ca_{1-x}Ba_xF_2$ layer, appearing as localized regions of enhanced intensity with lateral sizes of up to 100 nm. These local regions correlate well with the island sizes obtained from AFM surface maps (see Fig. 4 (d) of the manuscript), where the lateral dimensions of the islands range from 30 to 100 nm. Therefore, the dark-field TEM map in Fig. S2 (b) indicates the presence of locally barium-enriched regions within the $Ca_{1-x}Ba_xF_2$ layer. The highest-contrast regions may even correspond to BaF_2 (111) or BaF_2 (001) phase.

The linear contrast features observed within the layer $Ca_{1-x}Ba_xF_2$ in this map are most likely moire fringes, arising from the interference of diffracted electron waves associated with the different phases of $Ca_{1-x}Ba_xF_2$ and CaF_2 (or BaF_2) which have closely matched lattice parameters or a small mutual misorientation.

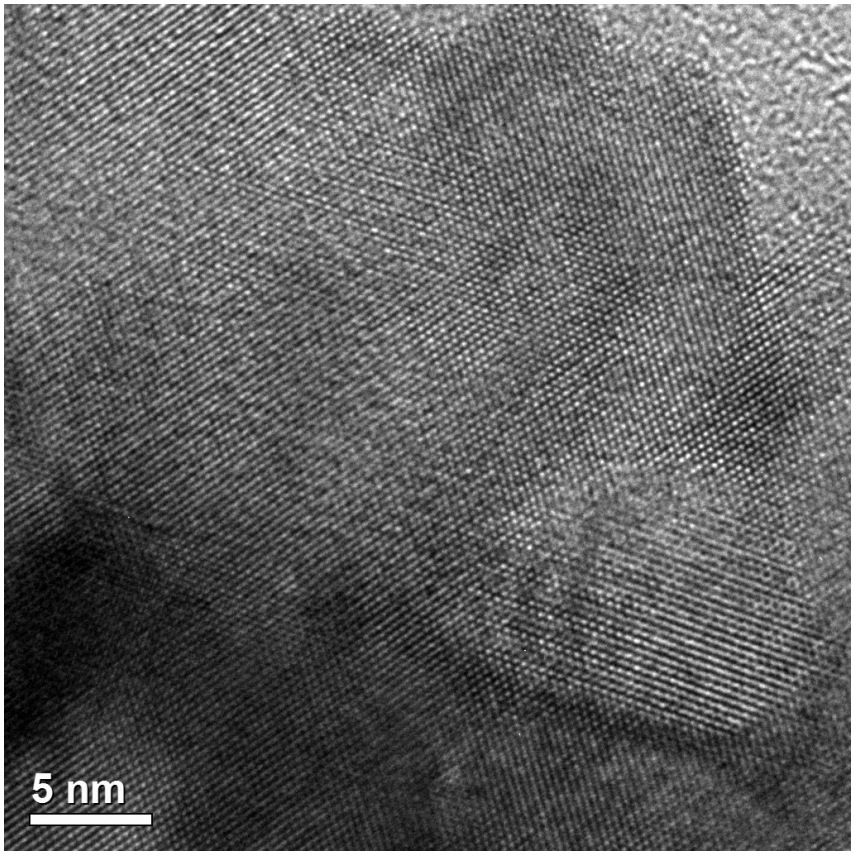

Fig. S6. HRTEM map of layer of Sample №6, with a solid solution growth temperature of 475°C, at the $Ca_{1-x}Ba_xF2/CaF2$ interface. The upper part of the image corresponds to $Ca_{1-x}Ba_xF_2$, and the lower part corresponds to the CaF_2 sublayer. The dark line indicates the interface.

Additionally, we plot an Arrhenius dependence ln(D) on T^{-1}(see Fig. S7 of Supplementary). Based on the obtained data for samples containing solid solution $Ca_{1-x}Ba_xF_2$ with stoichiometric coefficient x=0.375, the activation energy of diffusion E_a = 0.33 eV was estimated, and the critical radius of barium-enriched region nucleation r* was calculated (see Table S2 of Supplementary)."

Additionally, a semi-quantitative estimation of the diffusion coefficient was performed for samples containing the solid solution $Ca_{1-x}Ba_xF_2$ with stoichiometric coefficient x=0.375, the growth temperature of the solid solution layer for the samples under consideration was 300, 475, and 575°C. The estimation was based on the average lateral size of islands r and the growth time t, assuming a diffusion-limited mechanism:

$$D \approx \frac{r^2}{t}$$

Based on the obtained diffusion coefficient values, an Arrhenius curve—ln(D) versus 1/T—was shown in Fig. S7 of Supplementary.

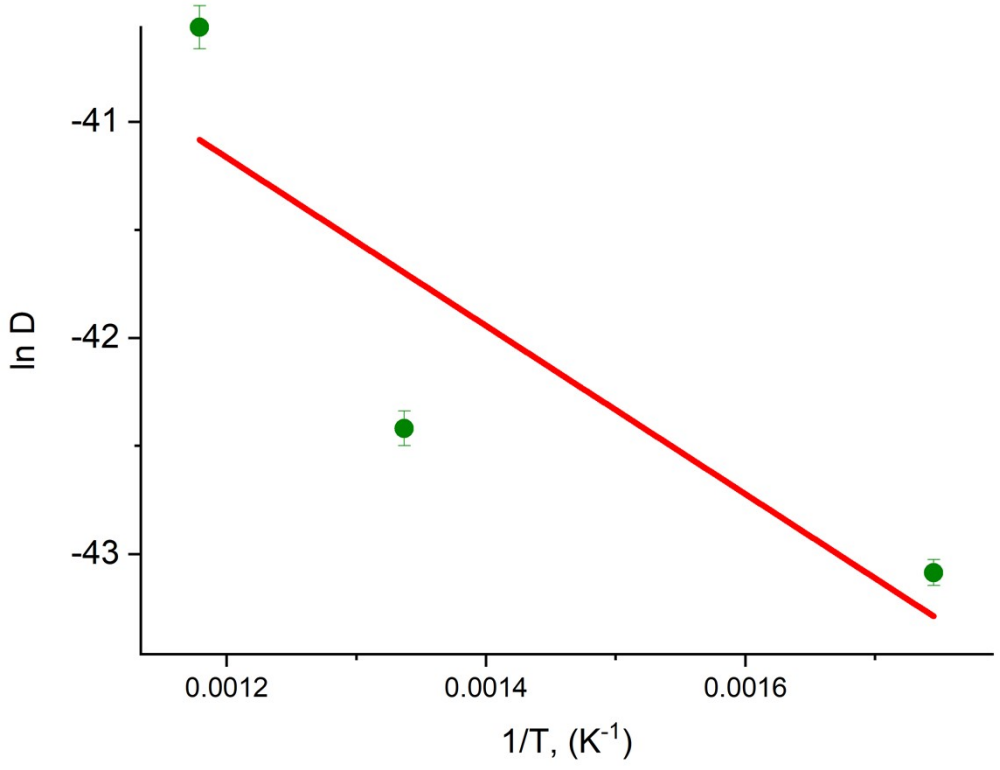

Fig. S7. Temperature dependence of the diffusion coefficient based on Arrhenius equation.

The activation energy analysis was performed according to the Arrhenius equation:

$$D(T) = D_0 \exp\left(-\frac{E_a}{kT}\right),$$

which in logarithmic form yields:

$$\ln(D) = lnD_0 - \frac{E_a 1}{k\,T}.$$

The activation energy of diffusion was determined from the slope of the linear approximation:

$$E_a = -mk,$$

where

$$m = \frac{\ln(D_1) - ln(D_2)}{\frac{1}{T_1} - \frac{1}{T_2}}.$$

As a result, the activation energy of diffusion was:

$E_a = 0.33eV$

The pre-exponential factor was:

$D_0 = 1.65 \cdot 10^{-16} m^2/s$

The obtained activation energy value falls within the range typical for ionic diffusion in fluoride solid solutions. According to Ref [45], the activation energy for F^- ion diffusion in the solid solution $Ca_{1-x}Ba_xF_2$ varies between 0.09–0.80 eV depending on the determination method and composition. Thus, the obtained value of 0.33 eV is consistent with literature data and can be considered realistic, despite the use of only three temperature points in plotting the curve in Fig. S7 and disregarding the nonlinearity of the dependence associated with changes in interatomic bond strengths in the material [46]. This supports the reasonableness of the Ba diffusion activation energy estimation in Ba-enriched regions within the adopted model.

To estimate the critical size of island nucleation, the interaction parameter Ω was calculated. It is assumed that the temperature of complete solid solution decomposition lies within the range of 600–700°C. In the calculations, Tc = 650°C (923 K) was adopted. The interaction parameter was determined from the relation according to [47]:

$\Omega = 2RT_c$

The bulk driving force for phase separation ΔG_V, associated with the Gibbs energy gain, was estimated at growth temperatures of 300, 475, and 575°C (573, 748, and 848 K, respectively) using the expression:

$$\Delta G_V \approx \frac{\Omega}{T_c V_m}(T_c - T),$$

where V_m – is the molar volume of the BaF_2 unit cell.

This molar volume was calculated according to the lattice parameter:

$$V_m = \frac{N_A \cdot a^3}{4},$$

where a is the lattice parameter value of the barium-enriched region (the BaF_2 lattice parameter value was used in the calculations).

The critical radius of the nucleus was estimated using the expression:

$$r^* = \frac{2\gamma}{|\Delta G_V|},$$

where γ – is the specific interfacial energy of the BaF_2 – vacuum boundary [47]. For BaF_2 the value γ=0.28 J/m^2 was adopted [48].

The calculated values of V_m, ΔG_V и r^* are presented in Table S2:

T, K	*Lattice parameter, A*	*V_m, cm^3/mol*	$\|\Delta G_V\|$, MJ/m^3	*r*, nm*	R_{min}, *nm*
573	*6.2*	*35.9*	*162.25*	*3.45*	*10*
748			*81.13*	*6.90*	*15*
848			*34.77*	*16.11*	*30*

Table S2 – Parameters used in the calculation of the critical nucleus radius r*. R_{min} – minimum lateral size of the island determined by atomic force microscopy.

The performed estimates of the critical size of barium-enriched region nucleation demonstrate correlation with experimental data: an increase in growth temperature is accompanied by a corresponding increase in the critical nucleation radius. The experimentally observed island sizes R_{min} exceed the calculated r*, values, which is due to the fact that the critical nucleus size itself is not measured, but rather the result of their subsequent lateral growth during the epitaxial process.

[45]. S. Breuer, M. Wilkening**,** Dalton Trans*.*, 2018, 47, p. 4105-4117

[46]. S. A Firstov, and G. F. Sarzhaz, Electron Microscopy and Strength of Materials, 2014, 20, p. 71–75.

Avaible at: https://nasplib.isofts.kiev.ua/server/api/core/bitstreams/17c82e70-4dc3-46ab-9db9-400abdca5d0e/content

[47]. J. W. Christian, The Theory of Transformations in Metals and Alloys, Pergamon Press, Oxford, 2002.

[48]. J. J. Gilman, *J. Appl. Phys., 1960, 31, p. 2208-2218.*